8-15-2006

Porous Fiber Formation in Polymer-Solvent System Undergoing Solvent Evaporation

Pratyush Dayal

Thein Kyu
University of Akron Main Campus, tkyu@uakron.edu

Porous fiber formation in polymer-solvent system undergoing solvent evaporation

Pratyush Dayal and Thein Kyu[a)]
Department of Polymer Engineering, University of Akron, Akron, Ohio 44325

(Received 4 January 2006; accepted 30 May 2006; published online 22 August 2006)

Temporal evolution of the fiber morphology during dry spinning has been investigated in the framework of Cahn-Hilliard equation [J. Chem. Phys. **28**, 258 (1958)] pertaining to the concentration order parameter or volume fraction given by the Flory-Huggins free energy of mixing [P. J. Flory, *Principles of Polymer Chemistry* (Cornell University Press, Ithaca, NY, 1953), p. 672] in conjunction with the solvent evaporation rate. To guide the solvent evaporation induced phase separation, equilibrium phase diagram of the starting polymer solution was established on the basis of the Flory-Huggins free energy of mixing. The quasi-steady-state approximation has been adopted to account for the nonconserved nature of the concentration field caused by the solvent loss. The process of solvent evaporation across the fiber skin-air interface was treated in accordance with the classical Fick's law [R. B. Bird *et al.*, *Transport Phenomena* (J. Wiley, New York, 1960), p. 780]. The simulated morphologies include gradient type, hollow fiber type, bicontinuous type, and host-guest type. The development of these diverse fiber morphologies is explicable in terms of the phase diagram of the polymer solution in a manner dependent on the competition between the phase separation dynamics and rate of solvent evaporation. © *2006 American Institute of Physics*.
[DOI: 10.1063/1.2259812]

INTRODUCTION

The porous fibers and membranes have been of immense interest because of their potential for applications in fuel cell membranes, drug delivery, electrochemical cells, chemical filtration, etc. Various porous membrane structures may be formed by thermally induced phase separation, air casting of polymer solutions, precipitation of vapor phase, immersion precipitation,[1–5] to name a few. During dry, wet, or electrospinning,[6–13] phase separated structures develop as the polymer solution undergoes solvent evaporation-induced phase separation into solvent-rich and polymer-rich regions depending upon the global and local thermodynamics as well as kinetic conditions. Specifically, the formation of these porous structures has been seemingly controlled by the competition between the phase separation dynamics and the solvent evaporation rate. The fiber (or membrane) appears porous as the solvent-rich phase is dried out.

The typical fiber morphologies observed experimentally during electrospinning[8–13] include the solid nanofiber, hollow tubes, ribbons, and beads. Recently, Casper *et al.*[14] reported that the electrospinning of polystyrene (PS) and tetrahydrofuran (THF) into the humid environment produces porous polymer nanofibers; the pore size and distribution are seemingly influenced by the molecular weight of polymer and percent humidity of the atmosphere. Water precipitation on the fiber surface was also presented as another possible account, but the authors attributed the formation of such pores on the fiber surface to phase separation associated with the penetration of water into the PS-THF solution. Recently, Liu and Kumar[15] reported the formation of porous microscopic polymer cups during the electrospinning of polymethylmethacrylate (PMMA)/nitromethane solution. However, when the electrospinning was undertaken in air from PMMA/methylene chloride solution, porous fibers were obtained. Their observation implies that environmental humidity may not be a necessary criterion for the formation of pores in electrospun nanofibers.

It has been postulated that the formation of porous fibers during electrospinning into the dry air environment is seemingly governed by solvent evaporation rate and phase separation kinetics. These processes are closely related to the thermodynamic phase diagram of the polymer solution. During the course of solvent evaporation, at a given temperature, the polymer concentration increases while passing through the coexistence regions such as metastable (nucleation and growth) regime and unstable spinodal regions. Hence, it is of paramount importance to first establish the equilibrium phase diagram of the polymer solution. In practice, however, the conditions in the solvent evaporation induced phase separation are far from equilibrium that depend on additional processes such as concentration, diffusivities of components, temperatures, etc., which certainly influence the evolved morphology. Thus, it is essential to understand the dynamics of microstructure formation within the emerged fiber and the influence of the aforementioned process variables on the final fiber morphologies. In this paper, we demonstrate how the resulting fiber morphologies are influenced by the competition between the dynamics of phase separation and the rate of solvent evaporation in relation to the equilibrium phase diagram.

[a)]Author to whom correspondence should be addressed; electronic mail: tkyu@uakron.edu

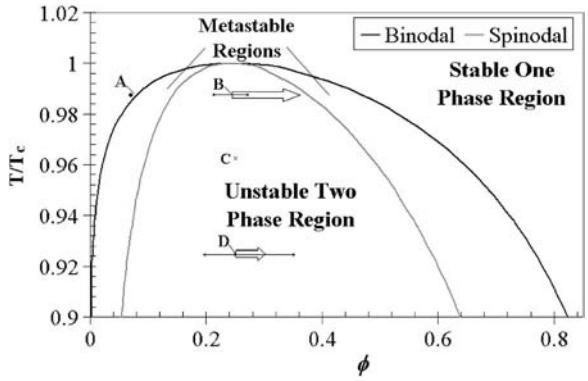

FIG. 1. A hypothetical equilibrium phase diagram for a polymer-solvent system with $n=10$ and $A=-4.5$. ϕ represents the polymer concentration.

ESTABLISHMENT OF PHASE DIAGRAM

Thermodynamic phase diagram of a polymer solution exhibiting an upper critical solution temperature (UCST) may be modeled in the framework of Flory-Huggins free energy of mixing, viz.,

$$F = \frac{\phi_1}{n} \ln \phi_1 + \phi_2 \ln \phi_2 + \chi_{12}\phi_1\phi_2, \tag{1}$$

where n is the statistical segment length of the constituent polymer, χ_{12} is the Flory-Huggins interaction parameter between the polymer and the solvent, and ϕ_1 and ϕ_2 are the volume fractions of polymer and solvent, respectively. The Flory-Huggins (FH) interaction parameter is given as usual $\chi_{12}=A+(\chi_c-A)T_c/T$, where A is the entropy correction factor, T is the absolute temperature, χ_c is the critical value of the FH interaction parameter given by $\chi_c=0.5(1+1/\sqrt{n})^2$, and T_c is the critical temperature. Setting $n=10$ and $A=-4.5$, a hypothetical UCST phase diagram was established (Fig. 1) by self-consistently solving the chemical potentials of each phase in conjunction with the common tangent method.

SOLVENT EVAPORATION INDUCED PHASE SEPARATION

The process of microstructure formation during electrospinning of a polymer solution is governed by the competition between the phase separation dynamics and the solvent evaporation rate. This process is generally described in the context of Cahn-Hilliard (CH) equation,[16,17] alternatively known as time-dependent Ginzburg-Landau (TDGL) (model B) equation,[18] coupled with the FH free energy of mixing.[19]

During the course of solvent evaporation, the polymer concentrations increase gradually due to the solvent loss through the fiber boundary. The dynamics of solvent escape across the boundary is expressed by Fick's equation[20] (see Appendix). As a result of the net loss of solvent mass from the boundary, the total volume of the fiber hence the fiber radius decreases. There is no doubt that the present hypothesis is too simplistic, but it is sufficient for the elucidation of emerged fiber morphology during solvent evaporation. With the knowledge of the diffusivity of solvent to surrounding air, the amount of solvent evaporated can be calculated and hence the change in volume of the fiber can be estimated. Based on the initial volume and the volume after the subsequent solvent loss, one can calculate the position of the interface provided that the fiber cross section remains circular.

According to the Cahn-Hilliard theory, the rate of change of polymer volume fraction ϕ_1 in time may be expressed in terms of the gradient of the chemical potentials in vector form (tilde sign signifies the vector operation) is given by

$$\frac{\partial\phi_1}{\partial t} = \tilde{\nabla} \cdot \Lambda_{12} \cdot \tilde{\nabla} \frac{\delta F}{\delta \phi_1}, \tag{2}$$

where the mutual diffusion coefficients are given according to the Onsager reciprocal relationship, i.e., $\Lambda_{12}=\Lambda_{0,11}\Lambda_{0,22}/(\Lambda_{0,11}+\Lambda_{0,22})$ with $\Lambda_{0,11}=\phi_1 n D_1$ and $\Lambda_{0,22}=(1-\phi_1)D_2$, where D_1 and D_2 are the self-diffusion coefficients of the polymer and the solvent, respectively.[18,21] In addition, the self-diffusion coefficient of the polymer is inversely proportional to the square of the number average molecular weight.[22–25]

The global free energy F may be described as the overall sum of the local free energy which may be given in accordance with the Flory-Huggins free energy[19] and the nonlocal interface gradient terms of de Gennes,[26]

$$F = \int_V \left\{ \frac{\phi_1}{n} \ln \phi_1 + \phi_2 \ln \phi_2 + \chi_{12}\phi_1\phi_2 + \frac{1}{36}\left(\frac{a_1^2}{\phi_1}|\tilde{\nabla}\phi_1|^2 + \frac{a_2^2}{\phi_2}|\tilde{\nabla}\phi_2|^2 \right) \right\} dV, \tag{3}$$

where a_1 and a_2 are the statistical segment lengths of the polymer and the solvent, respectively. For simplicity the elastic free energy arising from chain entanglements is neglected, although it can influence the diffusion process especially in the later stages of the drying process. Inserting (3) in (2) one obtains the Cahn-Hilliard equation in the following form, viz.,

$$\frac{\partial\phi_1}{\partial t} = \tilde{\nabla} \cdot \Lambda_{12} \tilde{\nabla} \left\{ \frac{1+\ln\phi_1}{n} - [1+\ln(1-\phi_1)] + \chi_{12}(1-2\phi_1) - \frac{1}{36}\left[\frac{a_1^2}{\phi_1^2} - \frac{a_2^2}{(1-\phi_1)^2} \right](\tilde{\nabla}\phi_1)^2 - \frac{1}{18}\left(\frac{a_1^2}{\phi_1} - \frac{a_2^2}{1-\phi_1} \right)(\nabla^2\phi_1) \right\}. \tag{4}$$

For a single phase system, polymer/good solvent in this case, the diffusion flux can be approximated to the gradient of the concentration instead of the gradient of the chemical potential which have a more general validity for both miscible or phase separating systems. As demonstrated in the Appendix, Fick's second law of diffusion[20] can be derived from the aforementioned assumption for describing the solvent evaporation process through the fiber boundary. In the absence of external flow, Fick's diffusion equation for the evaporation of solvent into air may be written as

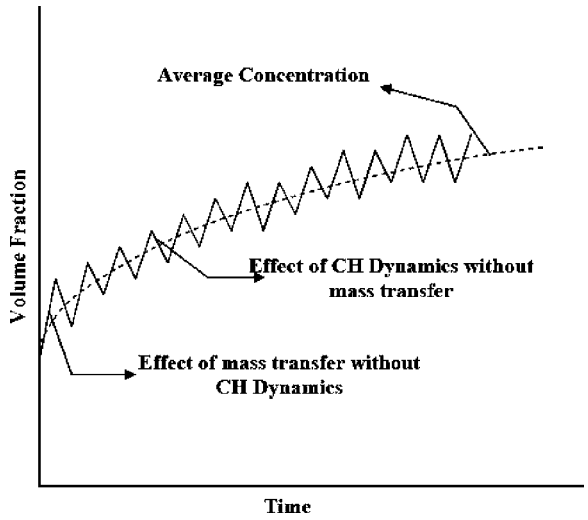

FIG. 2. Schematic diagram to illustrate the variation of concentration based on quasi-steady-state approximation (QSSA).

$$\frac{\partial \phi_2}{\partial t} = \alpha_0 \nabla^2 \phi_2, \tag{5}$$

where α_0 is the solvent diffusivity. Since solvent escapes through the outer boundary of the fiber to the infinite volume of surrounding air, the amount of solvent in air is negligible. The boundary layer is considered to be sharp with zero thickness for simplicity.

SIMULATION SCHEME

The numerical scheme form computing the local concentration field was implemented in the framework of quasi-steady-state approximation (QSSA) which is schematically represented in Fig. 2. At the beginning of every time step, say $t=t_0$, the volume fractions at the fiber boundary are modified due to the solvent loss. Thus, at the end of the time-step, $t=t_0$, the volume of the solvent inside the fiber has changed from v_s to v_s' while the volume of the polymer remains constant at v_p. The volume fraction of the polymer ϕ' at every point in fiber is updated using the relation $\phi'=v_p/(v_p+v_s)$. Subsequently, the volume fraction of the polymer is redistributed in the context of the standard Cahn-Hilliard time evolution or TDGL (model B) equation under the no flux boundary conditions. Equations (4) and (5) are solved numerically based on the finite difference method using second-order central differences in space and first-order forward difference in time. Initially the system consists of a cylindrical fiber with the boundaries being updated after each iteration. The cylindrical fiber elongates reflecting the shrinkage in the diameter of the fiber associated with the solvent loss. The simulation was performed on a fixed radial coordinate frame in dimensionless units and the calculated values were subsequently converted into the actual units by employing the material parameters. The initial distribution of polymer in the system was considered homogeneous, but the concentration fluctuation is introduced through thermal perturbation (or white noise) that obeys the fluctuation-dissipation theorem. The details of the simulation scheme are given elsewhere.[27]

RESULTS AND DISCUSSION

Figure 1 represents the standard equilibrium phase diagram for a polymer-solvent system based on the FH free energy of mixing. There are three distinct regions in the UCST phase diagram of a hypothetical polymer solution, viz., the stable single phase region, unstable two-phase region, and metastable regions. During solvent evaporation, the average polymer concentration increases and thus the system traverses across the phase diagrams by first passing through the metastable region. In this metastable region, phase separation is seemingly governed by the nucleation and growth mechanism. However, when the concentration continues to increase, the system transits from the metastable to unstable region in which the process of phase separation is dominated by spinodal decomposition (SD). The crossover from the nucleation and growth (NG) to spinodal decomposition is expected, although these two mechanisms of structure development may not be distinguishable in the late stages of the phase separation process. The crossover of NG to SD has been observed by our group, both experimentally and theoretically, in a polymerizing system. Here, no attempt has been made to verify the crossover phenomenon due to the very fast solvent evaporating rate. It is also not technically feasible to perform the *in situ* monitoring by synchrotron radiation during the electrospinning process. In addition, the nanofiber diameter is too small to achieve a reputable signal-to-noise ratio. When the system is quenched deeper to lower temperatures, the phase separation kinetics becomes faster relative the solvent evaporation rate. Hence for a given fixed simulation time, the domain size of the evolved structure would be larger at the lower temperatures. However, the shrinkage of the fiber diameter resulting from the solvent evaporation is not pronounced because most of the shrinkage during the actual spinning process takes place due to stretching.

To mimic the dynamics of the polymer solvent system undergoing solvent evaporation from the fiber boundary, the following parameters have been utilized: $\Lambda_{0,11}=1\times10^{-10}$ m^2/s, $\Lambda_{0,22}=1\times10^{-9}$ m^2/s, and $a=1\times10^{-7}$ m. The values of initial polymer concentration ϕ_0, solvent diffusivity α_0, and temperature T were varied in the simulations. The solvent evaporation rate and the phase separation kinetics may be varied by changing the temperature. When temperature is lowered, the solvent evaporation is slower, whereas the phase separation kinetics becomes faster. In order to exclusively alter the solvent evaporation rate at a given temperature, the experiment has to be carried out under the controlled environment, e.g., a partially closed system with a controlled lid. Alternatively, one can use a different volatile solvent having a comparable phase diagram. Hence, it is much simpler for experimentalists to change the temperature as a way of changing both phase separation kinetics and solvent evaporation rates.

Let us now examine the fiber morphologies with reference to the phase diagram (Fig. 1). Consider the system to be initially in the stable single phase region (at point A) with the parameters $\phi_0=0.07$, $T/T_c=0.9875$, and $\alpha_0/\Lambda=-1.0$. When the solvent evaporation raises the polymer concentration that

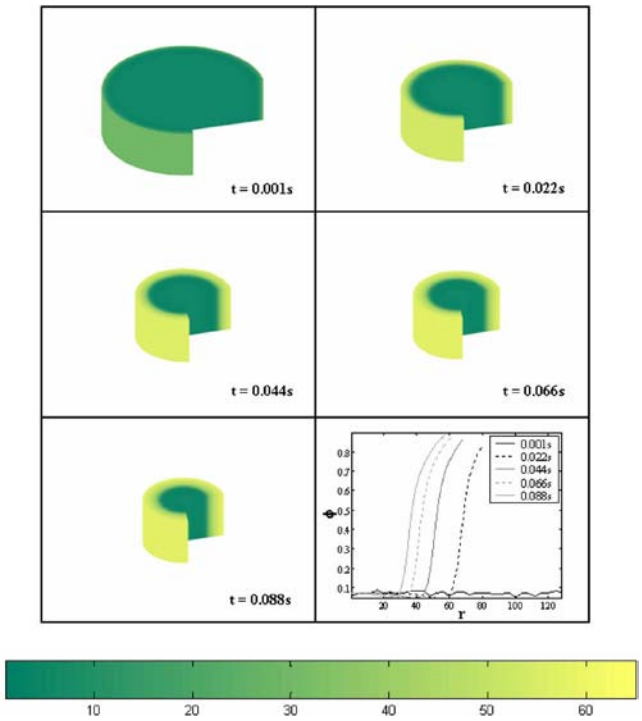

FIG. 3. Snapshots of a skin-core fiber morphology obtained at a very fast rate of solvent evaporation. The values in the color bar represent percentage composition of the polymer. The last image represents the concentration profile across the fiber radius.

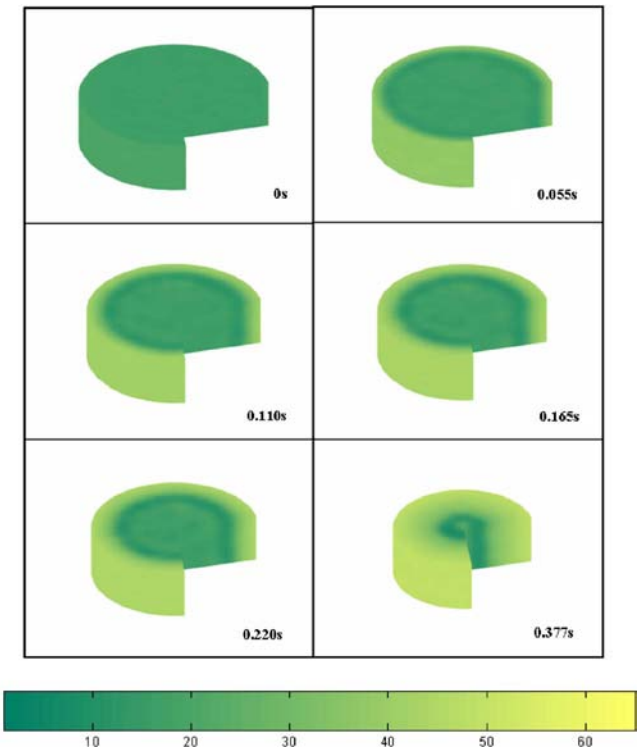

FIG. 4. Snapshots of a fiber cross section obtained at a fast rate of solvent evaporation, showing the initial phase separation followed by dissolution at the core. The values in the color bar represent percentage composition of the polymer.

eventually pushes the system into the unstable two-phase region, phase separation is expected to occur in a manner dependent on the relative rates of solvent evaporation and the phase separation. In the present case, by virtue of the fast solvent evaporation rate utilized, there is no discernible solvent evaporation induced phase separation (Fig. 3). Instead the development of the skin layer can be witnessed in which the polymer concentration is higher at the outer surface relative to the inner core. This observation is not surprising because the solvent evaporation is taking place exclusively from the boundary and thus the concentration fluctuations develop "outside in," resulting in the skin-core morphology, i.e., a hollow fiber. This type of morphology was reported by Guenthner *et al.*, when they performed two-dimensional (2D) simulations on a solvent evaporating system.[27]

To capture the effects of solvent evaporation induced phase separation, we have reduced the rate of solvent evaporation relative to that of phase separation ($\alpha_0/\Lambda=-0.1$) at point B in Fig. 1. We have also changed the initial polymer concentration to $\phi_0=0.25$ so that the system resides in the unstable two phase region to start with. In the time sequence of the system at point B (Fig. 4) we observe some structure evolution but as the time progresses the solvent evaporation drives the system further into the stable single phase region where the phase dissolution occurs. Some residual phase separated structures could be frozen by vitrification (due to the glassy nature of the constituent polymer) or chemical cross-linking (if the constituent polymer is reactive), but in this study we have neglected such effects for the sake of simplicity. Since the rate of solvent evaporation is relatively slow, the polymer solvent interface is not sharp and the emerged morphology is reminiscent of a gradient type showing gradual change in the polymer concentration across the fiber diameter. The qualitative analysis of the aforementioned observation implies that the evolved fiber morphology may be influenced by the interplay of phase separation and solvent evaporation rates.

To capture the effect of phase separation on the evolved fiber morphology, the temperature is dropped to $T/T_c=0.9625$ at point C (Fig. 1) to enhance the rate of phase separation. The snapshots of the emerging fiber structure are displayed in Fig. 5. The fiber morphology obtained under these conditions consists of a uniform polymer skin with a phase separated bicontinuous core. The bicontinuous microstructure thus formed is suggestive, although by no means a proof, of spinodal decomposition. Such bicontinuous phase is formed because the initial polymer concentration is in the vicinity of the critical polymer concentration ($\phi_c=0.24$) where SD is prevalent. This kind of cocontinuous morphology has been observed experimentally by Kyu *et al.*[28] when they extruded the 60% aqueous hydroxyl propyl cellulose (HPC) solution. It should be emphasized at this point that in all of the above cases the outer surface of the fiber is seemingly homogeneous because the outer skin, having the highest polymer concentration, may have existed from the two phase to the single phase region, and thus homogenization might have occurred at the outer fiber surface.

To obtain a porous fiber, it would be necessary to further reduce the relative rate of solvent evaporation to such an extent that would allow phase separation to occur at the fiber surface. To achieve this goal we have set $\alpha_0/\Lambda=-0.001$ and

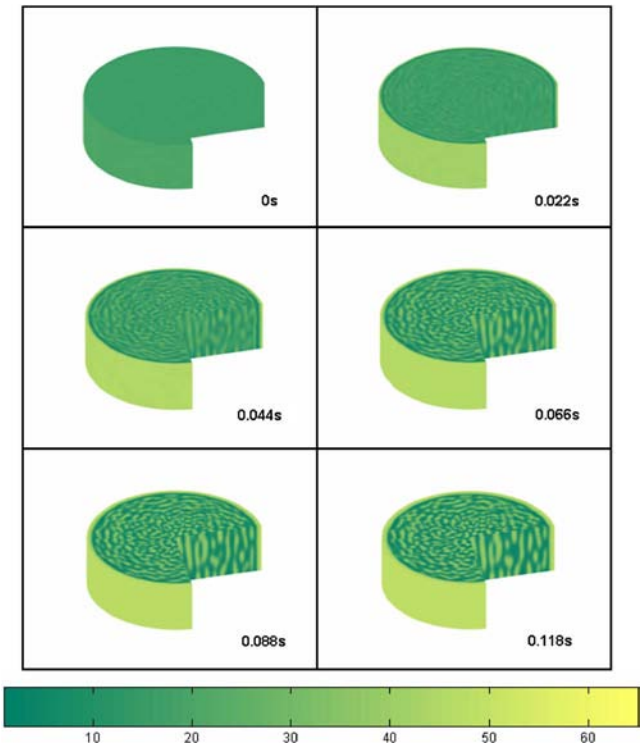

FIG. 5. Snapshots of a fiber cross section obtained at a slow rate of solvent evaporation, exhibiting a uniform outer surface with phase separated structures at the core. The values in the color bar represent percentage composition of the polymer.

$T/T_c=0.9250$ that corresponds to point D in Fig. 1. The time sequence of the porous fiber morphology is depicted in Fig. 6 showing the formation of pores at the skin. The pore structures may be attributed to phase separation through nucleation and growth, because the polymer concentration at the fiber surface is within the metastable gaps (65%). This type of skin-and-island morphology is akin to gel spun ultrahigh molecular weight polyethylene fibers as reported in literature.[29,30] Recently, Liu and Kumar[31] have also obtained this kind of morphology when they electrospun PMMA solution in methylenechloride.

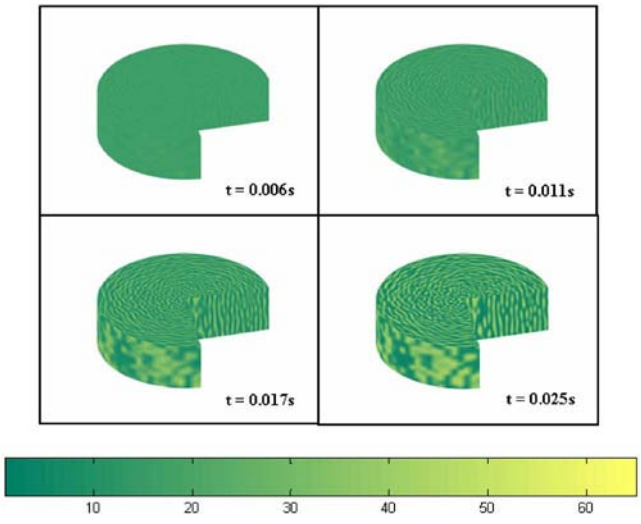

FIG. 6. Snapshots of a fiber cross section obtained at a very slow rate of solvent evaporation, exhibiting phase separated morphologies at the fiber surface as well as at the core. The values in the color bar represent percentage composition of the polymer.

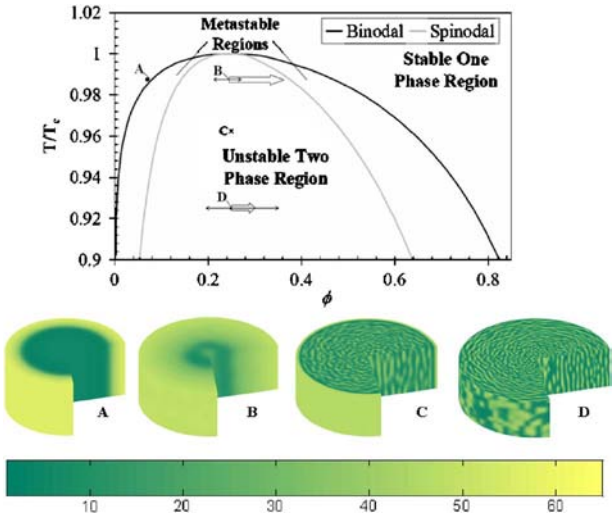

FIG. 7. Various fiber morphologies emerged from the points A–D within the phase diagram of the polymer-solvent system. The open arrow (⇒) indicates the direction of increasing polymer concentration due to the solvent evaporation, whereas the regular arrow (→) shows the direction of concentration field during phase separation. A: $\phi_0=0.07$ and $\alpha_0/\Lambda=-1.0$, B: $\phi_0=0.25$ and $\alpha_0/\Lambda=-0.1$, C: $\phi_0=0.25$ and $\alpha_0/\Lambda=-0.1$, and D: $\phi_0=0.25$ and $\alpha_0/\Lambda=-0.001$. The values in the color bar indicate the percent polymer concentration.

The fiber morphologies obtained from different starting conditions with reference to the phase diagram are summarized in Fig. 7 that includes the skin-core, uniform fiber surface with phase separated core, and porous fiber morphologies. Depending on concentration and temperature within the phase diagram, the relative rates of solvent evaporation and phase separation can be altered which in turn controls the emerging morphology. It may be concluded that the interplay between the solvent evaporation and the phase separation dynamics exerts profound effect on the resultant morphology of the nanofibers.

CONCLUSIONS

In summary, the present theoretical study demonstrates that it is possible to produce porous fibers by manipulating the relative rates of solvent evaporation (by choosing lesser volatile solvents) to phase separation (by choosing deeper quench depths) in reference to the phase diagram of a polymer solution. The formation of bicontinuous core and host-guest types of morphology can be attributed to the initial condition with respect to the phase diagram and when the phase separation process is dominant over the solvent evaporation. On the contrary, the hollow fiber with gradient morphology is developed when the solvent evaporation process dominates over the phase separation. When the rate of solvent evaporation is very fast, a very sharp interface develops forming the hollow fiber. These predicted fiber morphologies show strong resemblance to the experimental fiber morphologies reported.

ACKNOWLEDGMENTS

The support of the National Science Foundation (Grant No. DMR-0209272), the Ohio Board of Regents (Research Challenge Grant), and National Aeronautics and Space Administration (Grant No. NCC-1-02002) for this work is greatly appreciated. We would also like to thank Dr. A. J. Guenthner of U.S. Naval Air Warfare Center, China Lake, CA for his suggestions and helpful discussion.

APPENDIX: CORRELATION BETWEEN CAHN-HILLIARD EQUATION AND FICK'S SECOND LAW OF DIFFUSION EQUATION

The Cahn-Hilliard equation[16,17] for a two component system containing a polymer and a solvent may be given by

$$\frac{\partial \phi}{\partial t} = \tilde{\nabla} \cdot \Lambda \cdot \tilde{\nabla} \frac{\delta F}{\delta \phi}, \tag{A1}$$

where ϕ is the volume fraction of the polymer, Λ is the polymer-solvent mutual diffusivity, and $\delta/\delta\phi \equiv \partial/\partial\phi - \tilde{\nabla} \cdot \partial/\partial\tilde{\nabla}\phi$ is the functional derivative with respect to ϕ and its gradient. The global free energy (F) may be expressed as

$$F = \int_V (f_{\text{local}} + f_{\text{nonlocal}}) dV, \tag{A2}$$

where the local free energy density is given by

$$f_{\text{local}} = \frac{r}{2}\phi^2 + \frac{u}{4}\phi^4, \tag{A3}$$

and the nonlocal free energy density may be expressed through the interface gradient term, viz.,

$$f_{\text{nonlocal}} = \kappa(\nabla\phi)^2, \tag{A4}$$

where κ is the coefficient of the concentration gradient. Depending on the sign of coefficients the Landau expansion of (A3), the local free energy density exhibits a double well (if r is negative) for a phase separating system, but a single well (if r is positive) for phase dissolution representing a single phase system. At the polymer (fiber)-air interface, the interface boundary is very sharp with zero thickness, and there is no contribution of the interface gradient term to the total free energy, and thus the nonlocal free energy, i.e., (A4), can be ignored. To represent a single phase associated with phase dissolution, one can rewrite (A3) for the simplest case, setting $u=0$ (i.e., ignoring higher order terms),

$$f_{\text{local}} = \frac{r}{2}\phi^2. \tag{A5}$$

Inserting (A5) into (A1) and ignoring the gradient term, one obtains the following equation, setting $r=1$ and assuming a constant diffusivity Λ, i.e.,

$$\frac{\partial \phi}{\partial t} = \Lambda \nabla^2 \phi. \tag{A6}$$

Equation (A6) is nothing but Fick's second law of diffusion equation.[20] Essentially Fick's equation is a special case of the Cahn-Hilliard equation, and thus it should be valid for describing the solvent evaporation through the sharp fiber-air interface of zero thickness.

[1] H. Matsuyama, H. Okafuji, T. Maki, M. Teramoto, and N. Kubota, J. Membr. Sci. **223**, 119 (2003).
[2] M. Shang, H. Matsuyama, M. Teramoto, D. R. Lloyd, and N. Kubota, Polymer **44**, 7441 (2003).
[3] J. M. Saldanha and T. Kyu, Macromolecules **20**, 2840 (1987).
[4] C. Stropnik, and V. Kaiser, Desalination **145**, 1 (2002).
[5] P. van de Witte, P. J. Dijkstra, J. W. A. van den Berg, and J. Feijen, J. Membr. Sci. **117**, 1 (1996).
[6] J. M. Deitzel, J. Kleinmeyer, D. Harris, and N. C. Beck Tan, Polymer **42**, 261 (2001).
[7] J. M. Deitzel, W. Kosik, S. H. McKnight, N. C. Beck Tan, J. M. DeSimone, and S. Crette, Polymer **43**, 1025 (2002).
[8] H. Fong, I. Chun, and D. H. Reneker, Polymer **40**, 4585 (1999).
[9] J. Kameoka, and H. G. Craighead, Appl. Phys. Lett. **83**, 371 (2003).
[10] S. Koombhongse, W. Liu, and D. H. Reneker, J. Polym. Sci., Part B: Polym. Phys. **39**, 2598 (2001).
[11] K. H. Lee, H. Y. Kim, H. J. Bang, Y. H. Jung, and S. G. Lee, Polymer **44**, 4029 (2003).
[12] A. L. Yarin, A. G. Yazicioglu, and C. M. Megaridis, Appl. Phys. Lett. **86**, 013109 (2005).
[13] A. L. Yarin, A. G. Yazicioglu, C. M. Megaridis, M. Pia Rossi, and Y. Gogotsi, J. Appl. Phys. **97**, 124309 (2005).
[14] C. L. Casper, J. S. Stephens, N. G. Tassi, D. B. Chase, and J. F. Rabolt, Macromolecules **37**, 573 (2004).
[15] J. Liu and S. Kumar, Polymer **46**, 3211 (2005).
[16] J. W. Cahn, Acta Metall. **9**, 795 (1961).
[17] J. W. Cahn and J. E. Hilliard, J. Chem. Phys. **28**, 258 (1958).
[18] *Phase Transitions and Critical Phenomena*, edited by C. Domb and J. L. Lebowitz (Academic Press, New York, 2001), Vol. 19, p. 498.
[19] P. J. Flory, *Principles of Polymer Chemistry* (Cornell University Press, Ithaca, NY, 1953), p. 672.
[20] R. B. Bird, W. E. Stewart, and E. N. Lightfoot, *Transport Phenomena* (J. Wiley, New York, 1960), p. 780.
[21] P. Pincus, J. Chem. Phys. **75**, 1996 (1981).
[22] M. Doi and S. F. Edwards, J. Chem. Soc., Faraday Trans. 2 **74**, 1789 (1978).
[23] M. Doi and S. F. Edwards, J. Chem. Soc., Faraday Trans. 2 **74**, 1802 (1978).
[24] M. Doi and S. F. Edwards, J. Chem. Soc., Faraday Trans. 2 **74**, 1818 (1978).
[25] M. Doi and S. F. Edwards, J. Chem. Soc., Faraday Trans. 2 **75**, 38 (1979).
[26] P. G. De Gennes, J. Chem. Phys. **72**, 4756 (1980).
[27] A. J. Guenthner, S. Khombhongse, W. Liu, P. Dayal, and T. Kyu, Macromol. Theory Simul. **15**, 87 (2006).
[28] T. Kyu, P. Zhuang, and P. Mukherjee, ACS Symp. Ser. **384**, 266 (1989).
[29] M. Matsuo and R. S. J. Manley, Macromolecules **15**, 985 (1982).
[30] S. K. Roy, T. Kyu, and R. S. J. Manley, Macromolecules **21**, 499 (1988).
[31] J. Liu and S. Kumar (private communication).